



Short communication

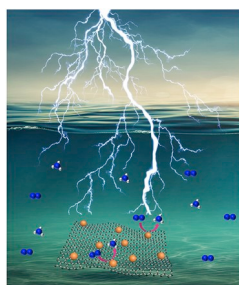
New insights into mechanisms on electrochemical N₂ reduction reaction driven by efficient zero-valence Cu nanoparticles

Xiaoxi Guo^a, Wencai Yi^c, Fengli Qu^{a,*}, Limin Lu^{b,**}^a College of Chemistry and Chemical Engineering, Qufu Normal University, Qufu, 273165, Shandong, China^b Institute of Functional Materials and Agricultural Applied Chemistry, College of Science, Jiangxi Agricultural University, Nanchang, 330045, China^c School of Physics and Physical Engineering, Qufu Normal University, Qufu, 273165, China

HIGHLIGHTS

- The Cu NPs-rGO was prepared via a facile two-step process.
- The Cu NPs-rGO was used as a NRR electrocatalyst under ambient conditions.
- Such electrocatalyst possesses marvelous NRR performance.
- Catalytic mechanism was investigated by density function theory calculations.

GRAPHICAL ABSTRACT



ARTICLE INFO

Keywords:

Electrocatalyst
N₂ reduction reaction
Cu NPs-rGO
Zero-valence
Ambient conditions
Density functional theory

ABSTRACT

Electrochemical N₂ reduction reaction (NRR) catalyzed by transition-metal-based electrocatalysts offers the sustainable strategy to directly convert N₂ to NH₃ at ambient conditions, but it is still extremely challenging for such catalysts to simultaneously obtain a high Faradaic efficiency (FE) and a large NH₃ yield. Herein, we report the zero-valence Cu nanoparticles anchored on reduced graphene oxide (Cu NPs-rGO) as a highly effective NRR electrocatalyst for ambient N₂-to-NH₃ conversion in a neutral solution. When measured in 0.5 M LiClO₄, the Cu NPs-rGO achieves a high Faradaic efficiency of 15.32% and a large NH₃ yield of 24.58 μg h⁻¹ mg_{cat}⁻¹ at -0.4 V vs. reversible hydrogen electrode. In addition, such electrocatalyst possesses marvelous stability and selectivity as well. The density functional theory calculations are carried out to further investigate the catalytic mechanism.

1. Introduction

Ammonia (NH₃), a vital industrial chemical, plays an indispensable role in agricultural, plastic, pharmaceutical and textile industries [1–5]. Intriguingly, NH₃ has been paid widespread attention owing to its low liquefying pressure, ideal hydrogen storage medium and carbon-free

characteristic [6–8]. At present, the NH₃ production mainly depends on the traditional Haber-Bosch process, in which N₂ and H₂ are coactivated by heterogeneous catalyst at high pressures (150–300 atm) and temperatures (300–500 °C) [9–12]. However, such process accounts for over 1% total global fossil energy and causes more than 300 million metric tons of CO₂ emissions annually [13,14], and thus economic and

* Corresponding author.

** Corresponding author.

E-mail addresses: fengliqun@hotmail.com (F. Qu), lulimin816@hotmail.com (L. Lu).<https://doi.org/10.1016/j.jpowsour.2019.227417>

Received 23 September 2019; Received in revised form 22 October 2019; Accepted 5 November 2019

Available online 12 November 2019

0378-7753/© 2019 Elsevier B.V. All rights reserved.

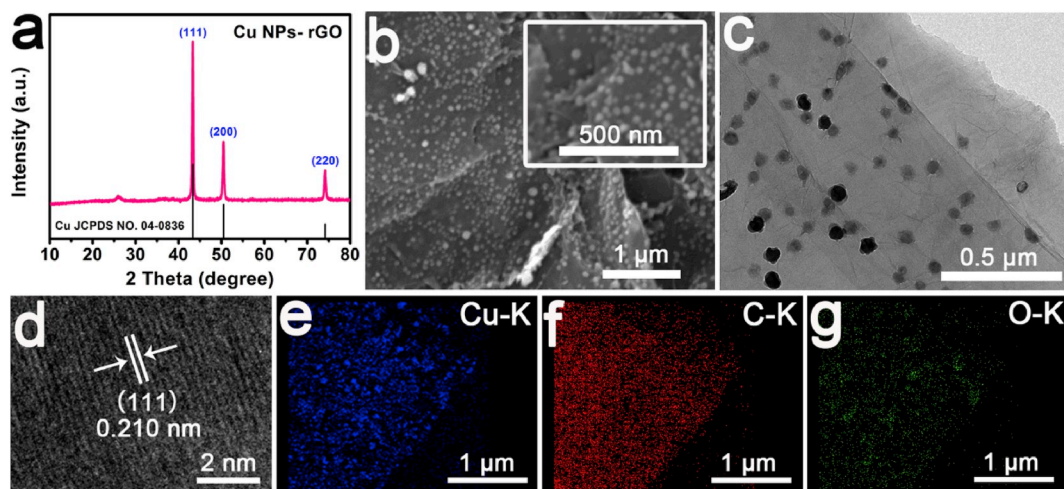


Fig. 1. (a) XRD pattern for Cu NPs-rGO. (b) SEM images and (c) TEM image of the Cu NPs-rGO. (d) HRTEM image taken from Cu NPs-rGO. EDX elemental mapping images of (e) Cu, (f) C and (g) O for Cu NPs-rGO.

sustainable alternatives are desired.

Electrocatalytic N_2 reduction under ambient conditions has great potential to achieve clean, carbon-free and sustainable NH_3 production from N_2 and H_2O directly, which is expected to be a good choice to replace Haber-Bosch process [15,16]. Most importantly, efficient electrocatalysts for N_2 reduction reaction (NRR) are vital parameter to it. Various noble metal-based catalysts have been reported as excellent NRR heterogeneous electrocatalysts due to their superb conduction, active polycrystalline surfaces, easy combination with reactants and so on, but their practical applications are limited by scarcity, high cost and low efficiency [17–20]. In this regard, developing novel strategies to elevate NRR activity of electrocatalysts, which are low-cost and earth-abundant, still remains challenging and alluring.

Cu, a cheap transition metal, which possesses appealing physical and chemical properties, has aroused great research interests. Cu-based materials can undergo a variety of reactions due to wide range of Cu's accessible valence states [21]. In general, the π backdonation role between metals and nitrogen weakens the $N\equiv N$ bond which is crucial in effective N_2 binding and activation [22]. Hence, zero-valence Cu catalysts can be compared favorably to oxidized Cu materials in forming π backdonation. On the other hand, the main challenge in developing catalytic zero-valence Cu nanoparticles (Cu NPs) is to synthesize nanomaterials which are highly active, stable, robust, and inexpensive. Anchoring Cu NPs on supports is an effective way to desolve it. Encouragely, graphene oxide (GO) has attracted numerous attention as a superior catalyst support due to its high specific surface area, excellent electrical conductivity and strong nanoparticle coupling [23,24]. Taking above concerns into account, we synthesized the zero-valence Cu nanoparticles anchored on reduced graphene oxide (Cu NPs-rGO) by hydrothermal method and H_2/Ar anneal treatment. As a superior NRR electrocatalyst for ambient N_2 -to- NH_3 conversion process, the as-obtained Cu NPs-rGO achieves a large NH_3 yield rate (V_{NH_3}) of $24.58 \mu g h^{-1} mg_{cat}^{-1}$ and a high Faradaic efficiency (FE) of 15.32% at $-0.4 V$ vs. reversible hydrogen electrode (RHE) in $0.5 M LiClO_4$. Moreover, such electrocatalyst exhibits high electrochemical stability and superior selectivity. Furthermore, density functional theory (DFT) calculations are used to explain NRR mechanism.

2. Experimental section

2.1. Preparation of Cu NPs-rGO powder, Cu NPs powder and rGO powder

0.5, 1.0, 1.5 and 2.0 mM $CuAc_2 \cdot H_2O$ with 50 mg graphene powder

dissolved in 35 mL H_2O , respectively, and ultrasonic treatment for 1 h. Then the solutions were transferred to 50 mL Teflon-lined autoclaves and heated to $180^\circ C$ for 2 h. When the autoclave naturally cooled down to room temperature, the autoclaves were taken out. The samples were obtained through centrifugation, washed with water for three times to remove unreacted $CuAc_2 \cdot H_2O$ and as-made powders were freeze drying for 24 h. Finally, the powders were annealed at $500^\circ C$ for 3 h under a mixture of Ar/H_2 flow. The Cu NPs powder and rGO powder were prepared according above method without adding graphene powder and $CuAc_2 \cdot H_2O$, respectively.

2.2. Preparation of Cu NPs-rGO/CP, Cu NPs/CP and rGO/CP electrodes

10 mg Cu NPs-rGO powder and 40 μL of Nafion solution (5 wt%) were dispersed in 960 μL mixed solution contain 640 μL ethanol and 320 $\mu L H_2O$ by 2 h sonication to form a homogeneous ink. Then, 10 μL Cu NPs-rGO was loaded on a piece of clean CP with area of $1.0 \times 1.0 cm^2$ and dried at room temperature. The Cu NPs/CP and rGO/CP electrodes were prepared according above method.

2.3. Computational details

Spin-polarized density functional theory (DFT) calculations were performed by using the plane wave-based Vienna ab initio simulation package (VASP) [25,26]. The generalized gradient approximation method with Perdew-Burke-Ernzerhof (PBE) functional was used to describe the exchange-correlation interaction among electrons [27]. The van der Waals (vdW) correction with the Grimme approach (DFT-D3) was included in the interaction between single molecule/atoms and substrates [28]. The energy cutoff for the plane wave-basis expansion was set to 400 eV and the atomic relaxation was continued until the forces acting on atoms were smaller than $0.01 eV \text{ \AA}^{-1}$. The Cu (111) surface was modeled using a 4×4 slab with three metal layers and the bottom trilayer is fixed, which is separated by 15 \AA of vacuum. The Brillouin zone was sampled with $3 \times 3 \times 1$ Gamma-center k-point mesh, and the electronic states were smeared using the Fermi scheme with a broadening width of 0.1 eV. The free energies of the reaction intermediates were obtained by $\Delta G = \Delta E_{ads} + \Delta ZPE - T\Delta S + \Delta G(U) + \Delta G(pH)$, where ΔE_{ads} is the adsorption energy, ZPE is the zero point energy and S is the entropy at 298 K. The effect of a bias was included in calculating the free energy change of elementary reactions involving transfer of electrons by adding $\Delta G(U) = -neU$, where n is number of electrons transferred and U is the electrode potential [29]. In our calculations, we used $U = -0.40 V$ (vs. RHE). $\Delta G(pH) = -k_B T \ln 10 \times pH$,

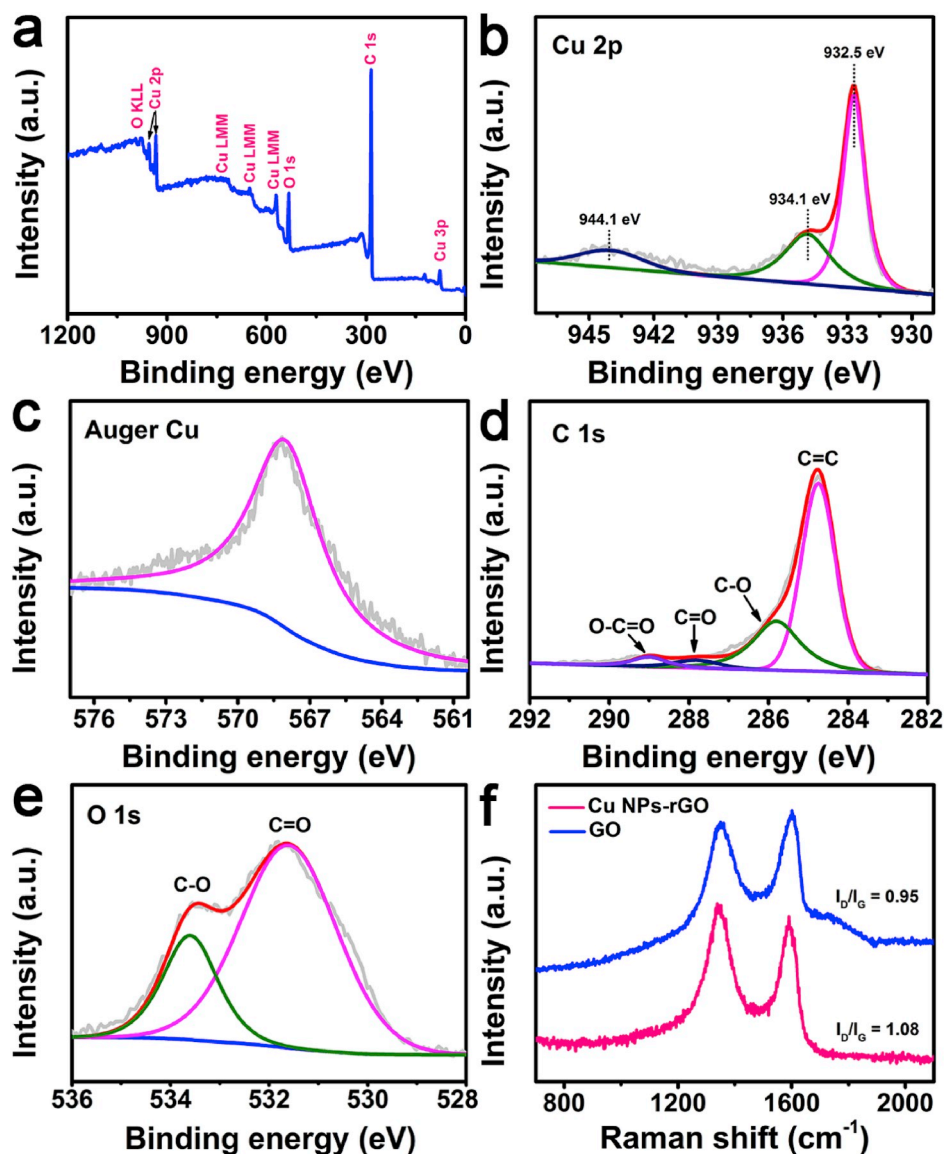


Fig. 2. (a) XPS survey spectrum of Cu NPs-rGO. High-resolution XPS spectra of (b) Cu 2p, (c) Auger Cu, (d) C 1s and (e) O 1s regions. (f) Raman spectra for Cu NPs-rGO and rGO.

where k_B is the Boltzmann constant, and $\text{pH} = 7$ for electrolyte. In this study, the entropies of molecules in the gas phase are obtained from the literature [30].

3. Results and discussion

To determine the phase composition, the X-ray powder diffraction (XRD) analysis was conducted (Fig. 1a). As observed, the diffraction peak located at 26.3° derives from rGO [31] and three strong signals at 43.2° , 50.4° and 74.1° are indexed to the (111), (200) and (220) planes of Cu NPs phase (JCPDS NO. 04-0836), respectively. In Fig. S1, the transmission electron microscopy (TEM) image of rGO shows its wrinkled and folded 2D morphology. The scanning electron microscopy (SEM) images (Fig. 1b) and TEM image (Fig. 1c) of Cu NPs-rGO powder demonstrate that the Cu NPs are dispersed on rGO uniformly. Furthermore, the high-resolution TEM (HRTEM) image of the as-made catalyst exhibits well-resolved lattice fringes with an interplanar distance of 0.210 nm, which is indexed to the (111) plane of Cu NPs. The TEM energy dispersive X-ray spectrometry (TEM-EDX) elemental mapping images (Fig. 1e–g) show the even distribution of Cu, C and O elements, indicating the Cu NPs supported on rGO can be successfully prepared by

a facile approach.

The X-ray photoelectron spectroscopy (XPS) analysis is used to gain more insight into the element valence state and examine chemical composition of electrocatalysts. As shown in Fig. 2a, the XPS survey spectrum further verifies the presence of Cu, C and O elements. In Cu 2p region (Fig. 2b), the signal appeared at 934.1 eV and the shake-up peak at 944.1 eV [32,33] stem from the inevitable oxidation of Cu to CuO. The sharp peak positioned at the binding energy (BE) of 932.5 eV could be assigned to Cu^0 or Cu^+ , which is attributed to the effect of particle size and surface coverage on the binding energy [33,34]. In order to identify the Cu^+ and Cu^0 species, the Auger Cu KLL spectrum was provided (Fig. 2c). The obvious peak centered at 568.0 eV corresponds to Cu^0 [35]. As displayed in Fig. 2d, a sharp peak at the BE of 284.7 eV is in good agreement with C=C bonds. In addition, another three signals at the BEs of 285.8 eV, 287.8 eV, and 289.0 eV, which can be assigned to C–C, C=O, and –COO– bonds, respectively [36,37]. In O 1s region (Fig. 2e), the two peaks at 531.6 eV and 533.4 eV are assigned to C=O and C–O, respectively [38,39]. The Cu NPs-rGO together with GO were characterized by Raman spectroscopy as well. In Fig. 2f, two apparent peaks were observed for all samples. One is the breathing modes of rings (D-band), the other is the E_{2g} phonon of sp^2 -bonded carbon atoms

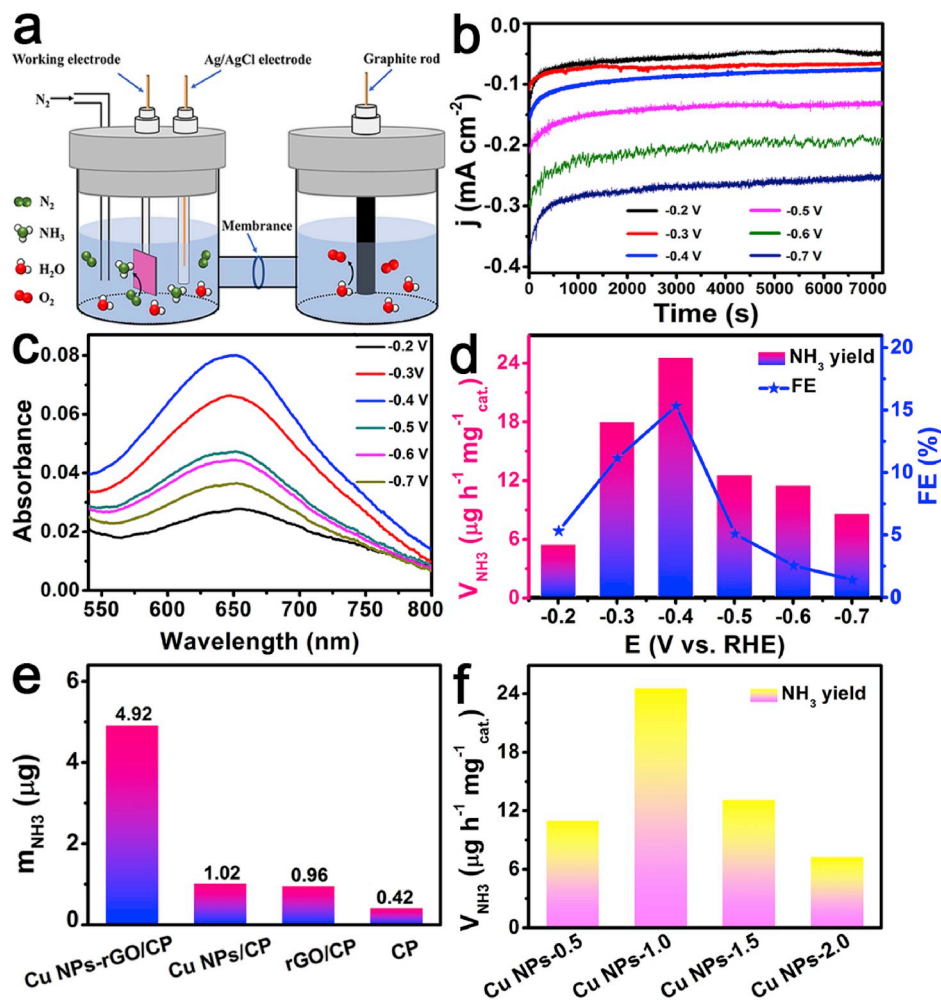


Fig. 3. (a) Schematic illustration of the NRR process. (b) Chronoamperometry measurements of the Cu NPs-rGO/CP at selected potentials in N_2 -saturated 0.5 M LiClO_4 . (c) UV-vis absorption spectra of the corresponding LiClO_4 electrolytes stained with indophenol indicator at various potentials for 7200 s. (d) V_{NH_3} and FEs at various potentials. (e) Amount of NH_3 over different electrodes at a potential of -0.4 V after electrolysis for 2 h. (f) V_{NH_3} of different Cu NPs loads at -0.4 V for 2 h.

(G-band) for carbon materials, and its intensity ratio of the D peak to G peak (I_D/I_G) is employed to investigate the change of GO. The I_D/I_G value of Cu NPs-rGO (1.08) is larger than that of GO (0.95), indicating the GO was reduced to rGO successfully.

Then, we explored the NRR activity of Cu NPs-rGO. The as-made Cu NPs-rGO electrocatalyst deposited on a piece of clean carbon paper (Cu NPs-rGO/CP, loading: 0.1 mg cm^{-2}) was employed as working electrode. As is exhibited in Fig. 3a, the NRR tests were performed in 0.5 M LiClO_4 aqueous solution using a H-type cell separated by Nafion 117 membrane under room temperature and atmospheric pressure. And the ultrahigh pure N_2 as feed gas was constantly purged into the cathode chamber for 30 min before electrolysis. All the potentials were reported on a RHE scale unless otherwise specified. The product NH_3 and the possible product N_2H_4 were spectrophotometrically determined adopting the indophenol blue method [40] as well as Watt and Chrisp method [41], respectively. Of note, the corresponding calibration curves are displayed in Fig. S2 and Fig. S3. As shown in Fig. 3b, the chronoamperometry measurements were conducted at different potentials from -0.2 V to -0.7 V for 7200 s. Then, the obtained electrolytes were collected and stained by indophenol indicator for 1 h. The relevant UV-vis absorption spectra are exhibited in Fig. 3c, and the highest absorbance intensity occurs at the applied potential of -0.4 V. The NH_3 yield (V_{NH_3}) and Faradaic efficiency (FE) at different potentials are shown in Fig. 3d. As observed, both V_{NH_3} and FE augment with the increasing negative potentials until -0.4 V. Subsequently, the outputs

and FEs decline at the same time, which is due to the competing hydrogen reaction reduction (HER) [42,43], a major side reaction that shuttles electrons and protons to generate H_2 and results in low FEs. Strikingly, the highest V_{NH_3} of $24.58 \mu\text{g h}^{-1} \text{mg}^{-1} \text{cat.}$ was obtained at -0.4 V with the highest FE of 15.32%, which are superior to those of most recent reported NRR electrocatalysts (Table S1). To identify the NH_3 outputs and FEs accurately, the produced NH_3 was determined via ion chromatography. The ion chromatogram curves at different applied potentials are displays in Fig. S4. And the obtained results from ion chromatography confirm the highest NH_3 yield is $23.46 \mu\text{g h}^{-1} \text{mg}^{-1} \text{cat.}$ with the FE of 12.53%, which are close to those from the indophenol blue method. Furthermore, there is no byproduct N_2H_4 to form (Fig. S5) after electrochemical NRR measurements which manifests the excellent selectivity of such catalyst. In order to verify the produced NH_3 is generated via N_2 reduction electrocatalyzed by Cu NPs-rGO, the relevant NRR experiments were further carried out under N_2 atmosphere with an open circuit and under Ar gas at -0.4 V for 7200 s. As observed in Fig. S6, the corresponding UV-vis spectra display weak absorption peaks, implying almost no NH_3 formation in both cases.

The NRR property of Cu NPs, rGO and bare carbon paper (CP) were also investigated at -0.4 V for 7200 s. As shown in Fig. 3e, the bare CP almost has no electrocatalytic performance. In the meantime, the Cu NPs/CP and rGO/CP have poor NRR performance with the low NH_3 outputs of 1.02 and 0.96 μg , respectively, compared to Cu NPs-rGO/CP (4.92 μg). In order to obtain the optimized activity, we probe the effect

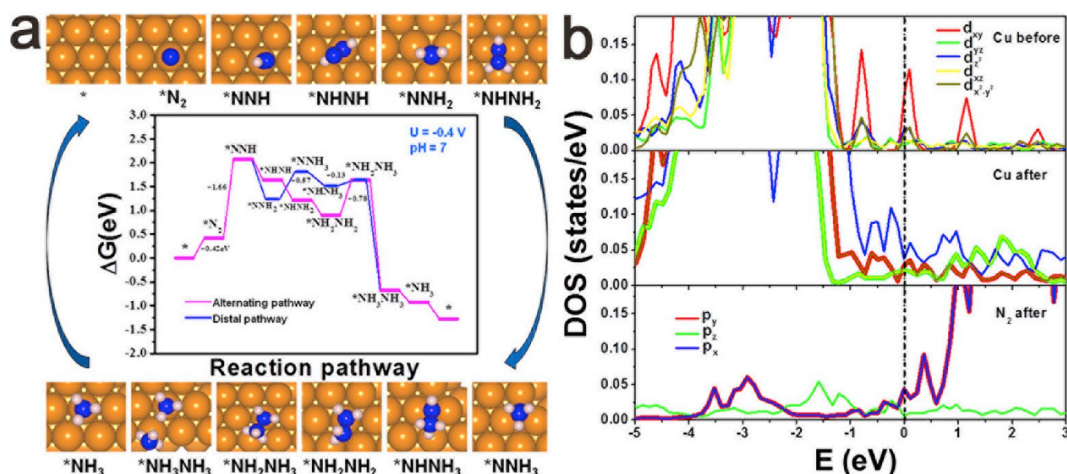


Fig. 4. (a) Free energy diagram of NRR on Cu (111) surface at $U = -0.40$ V. (b) DOS of Cu(111) surface before and after N_2 adsorption. Cu, brown; N, blue; H, white. (For interpretation of the references to colour in this figure legend, the reader is referred to the Web version of this article.)

of different Cu NPs loads on NRR performance. The 0.5, 1.0, 1.5 and 2.0 mM Cu NPs loads on rGO were defined as Cu NPs-0.5, Cu NPs-1.0, Cu NPs-1.5 and Cu NPs-2.0, respectively. In Fig. 3f, the highest V_{NH_3} was achieved by Cu NPs-1.0. Such results are attributed to the sizes of Cu particles. As observed in Figs. S7a and 7b, the SEM images of Cu NPs-0.5 and Cu NPs-1.0 demonstrate they have the similar particle size, but the Cu NPs-1.0 has larger Cu NPs load. The Cu NPs-1.5 and Cu NPs-2.0 with bigger particle sizes (Figs. S7c and 7d) cause less surface areas and active sites which are adverse to electrocatalysis. Moreover, it is striking to note that the rGO plays a critical role in N_2 fixation process. Firstly, the rGO with large surface areas are conducive to the dispersion of Cu NPs and prevent the agglomeration. Secondly, after hybrid of Cu NPs and rGO, the conductivity of Cu NPs has been improved remarkably (Fig. S8), which ensure efficient charge transfer to the active sites.

Stability is an essential parameter for catalysts. We studied the stability of such material through cycling stability test and long-term chronoamperometry measurement. In Fig. S9a, such catalyst was tested at -0.4 V for six time. Both the V_{NH_3} and FEs hardly decline during consecutive recycling tests. In the meantime, the Cu NPs-rGO/CP were measured at -0.4 V for at least 30 h and the current density shows no obvious decrease (Fig. S9b). Additionally, the XRD analysis after NRR test were also conducted. As displayed in Fig. S10, the XRD pattern shows that the peaks of Cu were still retained. In Fig. S11, the XPS spectra after long-term NRR test indicate that the main peak is located at 932.4 eV and chemical valence of Cu is still 0. On the basis of above results, the Cu NPs-rGO/CP possesses marvelous durability.

The good catalytic activity is closely related to the high electrochemical active surface areas (ECSAs) of catalysts, which can be assessed by the double layer capacitance (C_{dl}). And the cyclic voltammetry of different Cu NPs loads which was used to investigate C_{dl} with different scan rates at the region of -0.05 to 0.05 V were measured, where the current response was only due to the charging and recharging from the double layer (see Fig. S12 for more details). As exhibited, the Cu NPs-1.0 possesses the highest C_{dl} value (14.42 mF cm^{-2}) compared to those of Cu NPs-0.5 (11.04 mF cm^{-2}), Cu NPs-1.5 (14.27 mF cm^{-2}) and Cu NPs-2.0 (10.35 mF cm^{-2}), revealing the Cu NPs-1.0 has the highest ECSAs and equips with more active site.

Based on experiment observation, Cu (111) surface is mainly exposed. Thus, we consider NRR process on this surface. N_2 adsorption on Cu (111) surface has three possible sites (Fig. S13a), including top, hcp, and fcc, and calculation results show that N_2 molecule prefers to adsorb on top site by end-on coordination with free energy change of 0.42 eV ($\Delta G = 0.42 \text{ eV}$), as shown in Figs. S13b and 4a. Bader charge analysis shows that $*N_2$ is transferred into $0.09 e^-$, underlying it is effectively activated. Density of states (DOS) further demonstrates that

after N_2 adsorption, there are hybridizations between Cu 3d and N 2p around Fermi energy in Fig. 4b, which corresponds to π backdonation and σ donation. In general, the hydrogenation of N_2 is carried out by adding H atoms one by one to the adsorbed species with a distal or alternating mechanism. Our calculations show that the hydrogenation of N_2 to $*NNH$ experiences an uphill pathway with $\Delta G = 1.66 \text{ eV}$ in Fig. 4a. Then, the $*NNH$ to $*NNH_2$ or $*NHNH$ are downhill pathway, and the former, $*NNH$ to $*NNH_2$ process, is preferable due to a higher energy releasing. Then, the $*NNH_2$ to $*NNH_3$ is an uphill pathway with $\Delta G = 0.57 \text{ eV}$, but $*NHNH$ to $*NHNH_2$ is downhill pathway. As is hydrogenated to fifth hydrogen atom, the alternating ($*NH_2NH_2$ to $*NH_2NH_3$) and distal pathways ($*NHNH_3$ to $*NH_2NH_3$) are uphill with $\Delta G = 0.78$ and 0.13 eV , respectively. Subsequently, the process of $*NH_2NH_3$ to $*NH_3NH_3$ is quickly downhill. Surprisingly, all of NH_3 desorption processes are downhill pathway, indicating that Cu (111) surface is advantage to NH_3 gas formation. Above calculation results demonstrate that Cu (111) surface can effectively activate N_2 molecule and promote NH_3 desorption, which explains why this surface has good NRR performance. In the whole NRR process, the rate-determining step is controlled by the process of $*N_2$ to $*NNH$.

4. Conclusion

In summary, we find that the Cu NPs-rGO is a highly effective electrocatalyst for N_2 fixation under ambient conditions, which was well confirmed by experiment and theoretical calculation. Such catalyst attains a high Faradaic efficiency of 15.32% and a large NH_3 yield of $24.58 \mu\text{g h}^{-1} \text{ mg}_{\text{cat}}^{-1}$ at -0.4 V . The marvelous performance is attribute to the uniform distribution of Cu nanoparticles which exposes more active site, and the good conductivity of the hybrid which ensures the efficient charge transfer to the active sites. DFT calculation results demonstrate that Cu (111) surface can effectively activate N_2 molecule and the rate-determining step in the whole NRR process is controlled by the process of $*N_2$ to $*NNH$. This research not only provides us an effective NRR electrocatalyst, but also opens an intriguing new avenue to rational design of non-noble-based catalysts for artificial N_2 fixation.

Declaration of competing interest

We declare that we have no financial and personal relationships with other people or organizations that can inappropriately influence our work, there is no professional or other personal interest of any nature or kind in any product, service and/or company that could be construed as influencing the position presented in, or the review of, the manuscript entitled.

Acknowledgment

This work was supported by the National Natural Science Foundation of China (21775089, 51862014, 21665010), Outstanding Youth Foundation of Shandong Province (ZR2017JL010), the Key Research and Development Program of Jining City (2018ZDGH032) and Taishan scholar of Shandong Province.

Appendix A. Supplementary data

Supplementary data to this article can be found online at <https://doi.org/10.1016/j.jpowsour.2019.227417>.

References

- [1] V. Smil, Detonator of the population explosion, *Nature* 400 (1999) 415.
- [2] T. Vegge, R.Z. Sørensen, A. Klerke, J.S. Hummelshøj, T. Johannessen, J.K. Nørskov, C.H. Christensen, in: G. Walker (Ed.), *Solid-State Hydrogen Storage: Materials and Chemistry*, Woodhead Publishing, Cambridge, UK, 2008, pp. 533–564.
- [3] V. Rosca, M. Duca, M.T. de Groo, M.T.M. Koper, Nitrogen cycle electrocatalysis, *Chem. Rev.* 109 (2009) 2209–2244.
- [4] X. Guo, H. Du, F. Qu, J. Li, Recent progress in electrocatalytic nitrogen reduction, *J. Mater. Chem. A* 7 (2019) 3531–3543.
- [5] R. Schlögl, Catalytic synthesis of ammonia—A "Never-Ending story"? *Angew. Chem. Int. Ed.* 42 (2003) 2004–2008.
- [6] X. Cui, C. Tang, Q. Zhang, A review of electrocatalytic reduction of dinitrogen to ammonia under ambient conditions, *Adv. Energy Mater.* 8 (2018) 1800369.
- [7] J. Guo, P. Chen, Catalyst: NH_3 as an energy carrier, *Chem* 3 (2017) 709–714.
- [8] C. Liu, Q. Li, C. Wu, J. Zhang, Y. Jin, D.R. MacFarlane, C. Sun, Single-boron catalysts for nitrogen reduction reaction, *J. Am. Chem. Soc.* 141 (2019) 2884–2888.
- [9] X. Zhang, R. Kong, H. Du, L. Xia, F. Qu, Highly efficient electrochemical ammonia synthesis via nitrogen reduction reactions on a VN nanowire array under ambient conditions, *Chem. Commun.* 54 (2018) 5323–5325.
- [10] S. Mukherjee, D.A. Cullenb, S. Karakalosc, K. Liud, H. Zhang, S. Zhao, H. Xu, K. L. More, G. Wang, G. Wu, Metal-organic framework-derived nitrogen-doped highly disordered carbon for electrochemical ammonia synthesis using N_2 and H_2O in alkaline electrolytes, *Nano Energy* 48 (2018) 217–226.
- [11] P.J. Chirik, Nitrogen fixation: one electron at a time, *Nat. Chem.* 1 (2009) 520–522.
- [12] V. Kyriakou, I. Garagounis, E. Vasileiou, A. Vourros, M. Stoukides, Progress in the electrochemical synthesis of ammonia, *Catal. Today* 286 (2017) 2–13.
- [13] C. Guo, J. Ran, A. Vasileff, S. Qiao, Rational design of electrocatalysts and photo (electro) catalysts for nitrogen reduction to ammonia (NH_3) under ambient conditions, *Energy Environ. Sci.* 11 (2018) 45–56.
- [14] C.J.M. van der Ham, M.T.M. Koper, D.G.H. Hetterscheid, Challenges in reduction of dinitrogen by proton and electron transfer, *Chem. Soc. Rev.* 43 (2014) 5183–5191.
- [15] T. Wu, W. Kong, Y. Zhang, Z. Xing, J. Zhao, T. Wang, X. Shi, Y. Luo, X. Sun, Greatly enhanced electrocatalytic N_2 reduction on TiO_2 via V doping, *Small Methods* (2019), <https://doi.org/10.1002/smt.201900356>.
- [16] H. Du, X. Guo, R. Kong, F. Qu, Cr_2O_3 nanofiber: a high-performance electrocatalyst toward artificial N_2 fixation to NH_3 under ambient conditions, *Chem. Commun.* 54 (2018) 12848–12851.
- [17] H. Wang, Y. Li, C. Li, K. Deng, Z. Wang, Y. Xu, X. Li, H. Xue, L. Wang, One-pot synthesis of bi-metallic PdRu tripods as an efficient catalyst for electrocatalytic nitrogen reduction to ammonia, *J. Mater. Chem. A* 7 (2019) 801–805.
- [18] M. Shi, D. Bao, B. Wulan, Y. Li, Y. Zhang, J. Yan, Q. Jiang, Au sub-nanoclusters on TiO_2 toward highly efficient and selective electrocatalyst for N_2 conversion to NH_3 at ambient conditions, *Adv. Mater.* 29 (2017) 1606550.
- [19] M. Nazemi, S.R. Panikkanvalappila, M.A. El-Sayed, Enhancing the rate of electrochemical nitrogen reduction reaction for ammonia synthesis under ambient conditions using hollow gold nanocages, *Nano Energy* 49 (2018) 316–323.
- [20] Z. Wang, Y. Li, H. Yu, Y. Xu, H. Xue, X. Li, H. Wang, L. Wang, Ambient electrochemical synthesis of ammonia from nitrogen and water catalyzed by flower-like gold microstructures, *ChemSusChem* 11 (2018) 3480–3485.
- [21] M.B. Gawande, A. Goswami, F. Felpin, T. Asefa, X. Huang, R. Silva, X. Zou, R. Zboril, R.S. Varma, Cu and Cu-based nanoparticles: synthesis and applications in catalysis, *Chem. Rev.* 116 (2016) 3722–3811.
- [22] M.-A. Lègaré, G. Bélanger-Chabot, R.D. Dewhurst, E. Welz, I. Krummenacher, B. Engels, H. Braunschweig, Nitrogen fixation and reduction at boron, *Science* 359 (2018) 896–900.
- [23] C. Liu, H. Zhang, Y. Tang, S. Luo, Controllable growth of graphene/Cu composite and its nanoarchitecture-dependent electrocatalytic activity to hydrazine oxidation, *J. Mater. Chem. A* 2 (2014) 4580–4587.
- [24] A.K. Geim, K.S. Novoselov, Detection of individual gas molecules adsorbed on graphene, *Nat. Mater.* 6 (2007) 183–191.
- [25] G. Kresse, J. Furthmüller, Efficiency of ab-initio total energy calculations for metals and semiconductors using a plane-wave basis set Efficiency of ab-initio total energy calculations for metals and semiconductors using a plane-wave basis setComp, *Mater. Sci.* 6 (1996) 15–50.
- [26] G. Kresse, J. Furthmüller, Efficient iterative schemes for ab initio total-energy calculations using a plane-wave basis set, *Phys. Rev. B* 54 (1996) 11169.
- [27] J.P. Perdew, K. Burke, M. Ernzerhof, Generalized gradient approximation made simple, *Phys. Rev. Lett.* 77 (1996) 3865–3868.
- [28] S. Grimme, J. Antony, S. Ehrlich, H. Krieg, A consistent and accurate ab initio parametrization of density functional dispersion correction (DFT-D) for the 94 elements H-Pu, *J. Chem. Phys.* 132 (2010) 154104.
- [29] X. Zhang, T. Wu, H. Wang, R. Zhao, H. Chen, T. Wang, P. Wei, Y. Luo, Y. Zhang, X. Sun, Boron nanosheet: an elemental two-dimensional (2D) material for ambient electrocatalytic N_2 -to- NH_3 fixation in neutral media, *ACS Catal.* 9 (2019) 4609–4615.
- [30] <https://janaf.nist.gov/>. June 2019.
- [31] S.N. Alam, N. Sharma, L. Kumar, Synthesis of graphene oxide (GO) by modified hummers method and its thermal reduction to obtain reduced graphene oxide (rGO), *Graphene* 6 (2017) 1–18.
- [32] A.A. Dubale, C. Pan, A.G. Tamirat, H. Chen, W. Su, C. Chen, J. Rick, D. Worku Ayele, B.A. Aragaw, J. Lee, Y. Yang, B. Hwang, Heterostructured $\text{Cu}_2\text{O}/\text{CuO}$ decorated with nickel as a highly efficient photocathode for photoelectrochemical water reduction, *J. Mater. Chem. A* 3 (2015) 12482–12499.
- [33] J. Li, Z. Zhang, Y. Ji, Z. Jin, S. Zou, Z. Zhong, F. Su, One-dimensional Cu-based catalysts with layered $\text{Cu-Cu}_2\text{O-CuO}$ walls for the Rochow reaction, *Nano Res.* 9 (2016) 1377–1392.
- [34] Y. Wang, Y. Lu, W. Zhan, Z. Xie, Q. Kuang, L. Zheng, Synthesis of porous $\text{Cu}_2\text{O}/\text{CuO}$ cages using Cu-based metal-organic frameworks as templates and their gas-sensing properties, *J. Mater. Chem. A* 3 (2015) 12796–12803.
- [35] I. Platzman, R. Brenner, H. Haick, R. Tannenbaum, Oxidation of polycrystalline copper thin films at ambient conditions, *J. Phys. Chem. C* 112 (2008) 1101–1108.
- [36] V.K. Singh, A. Shukla, M.K. Patra, L. Saini, R.K. Jani, S.R. Vadera, N. Kumar, Microwave absorbing properties of a thermally reduced graphene oxide/nitrile butadiene rubber composite, *Carbon* 50 (2012) 2202–2208.
- [37] H. Chen, X. Zhu, H. Huang, H. Wang, Ting Wang, R. Zhao, H. Zheng, A.M. Asiri, Y. Luo, X. Sun, Sulfur dots-graphene nanohybrid: a metal-free electrocatalyst for efficient N_2 -to- NH_3 fixation under ambient conditions, *Chem. Commun.* 55 (2019) 3152–3155.
- [38] Z. Lu, G. Chen, S. Siahrostami, Z. Chen, K. Liu, J. Xie, L. Liao, T. Wu, D. Lin, Y. Liu, T.F. Jaramillo, J.K. Nørskov, Y. Cui, High-efficiency oxygen reduction to hydrogen peroxide catalysed by oxidized carbon materials, *Nat. Catal.* 1 (2018) 156–162.
- [39] S. Kundu, Y. Wang, W. Xia, M. Muhler, Thermal stability and reducibility of oxygen-containing functional groups on multiwalled carbon nanotube surfaces: a quantitative high-resolution XPS and TPD/TPR study, *J. Phys. Chem. C* 112 (2008) 16869–16878.
- [40] D. Zhu, L. Zhang, R.E. Ruther, R.J. Hamers, Photo-illuminated diamond as a solid-state source of solvated electrons in water for nitrogen reduction, *Nat. Mater.* 12 (2013) 836–841.
- [41] G.W. Watt, J.D. Chrisp, Spectrophotometric method for determination of hydrazine, *Anal. Chem.* 24 (1952) 2006–2008.
- [42] H. Du, R. Kong, F. Qu, L. Lu, Enhanced electrocatalysis for alkaline hydrogen evolution by Mn doping in a Ni_3S_2 nanosheet array, *Chem. Commun.* 54 (2018) 10100–10103.
- [43] J. Tian, Q. Liu, A.M. Asiri, X. Sun, Self-supported nanoporous cobalt phosphide nanowire arrays: an efficient 3D hydrogen-evolving cathode over the wide range of pH 0–14, *J. Am. Chem. Soc.* 136 (2014) 7587–7590.